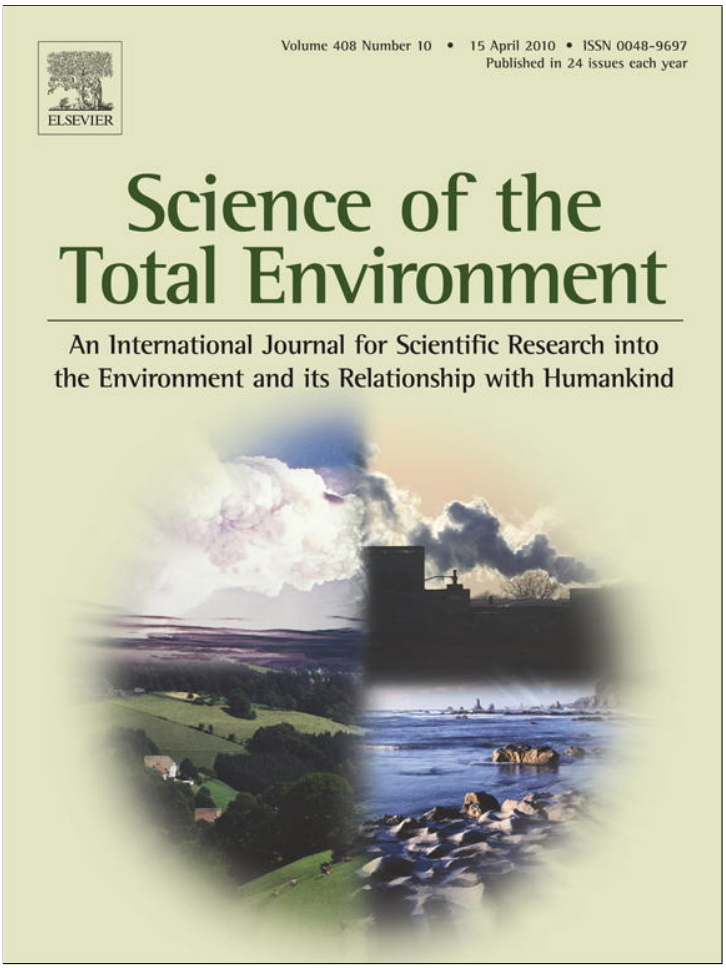

Science of the Total Environment 408 (2010) 2273–2282

Contents lists available at ScienceDirect

Science of the Total Environment

journal homepage: www.elsevier.com/locate/scitotenv

High yield combustion synthesis of nanomagnesia and its application for fluoride removal

Shihabudheen M. Maliyekkal, Anshup, K.R. Antony, T. Pradeep *

DST Unit on Nanoscience (DST UNS), Department of Chemistry and Sophisticated Analytical Instrument Facility, Indian Institute of Technology Madras, Chennai 600 036, India

ARTICLE INFO

Article history:
Received 5 August 2009
Received in revised form 8 October 2009
Accepted 25 January 2010
Available online 23 February 2010

Keywords:
Adsorption
Combustion synthesis
Defluoridation
Drinking water
Nanomagnesia
Nanoparticles

ABSTRACT

We describe a novel combustion synthesis for the preparation of Nanomagnesia (NM) and its application in water purification. The synthesis is based on the self-propagated combustion of the magnesium nitrate trapped in cellulose fibers. Various characterization studies confirmed that NM formed is crystalline with high phase purity, and the particle size varied in the range of 3–7 nm. The fluoride scavenging potential of this material was tested as a function of pH, contact time and adsorbent dose. The result showed that fluoride adsorption by NM is highly favorable and the capacity does not vary in the pH range usually encountered in groundwater. The effects of various co-existing ions usually found in drinking water, on fluoride removal were also investigated. Phosphate was the greatest competitor for fluoride followed by bicarbonate. The presence of other ions studied did not affect the fluoride adsorption capacity of NM significantly. The adsorption kinetics followed pseudo-second-order equation and the equilibrium data are well predicted by Frendlich equation. Our experimental evidence shows that fluoride removal happened through isomorphic substitution of fluoride in brucite. A batch household defluoridation unit was developed using precipitation–sedimentation–filtration techniques, addressing the problems of high fluoride concentration as well as the problem of alkaline pH of the magnesia treated water. The method of synthesis reported here is advantageous from the perspectives of small size of the nanoparticle, cost-effective recovery of the material and improvement in the fluoride adsorption capacity.

1. Introduction

Magnesium oxide (MgO) is an important material for various applications including catalysis, waste remediation, additives in refractory and paint products (Ding et al., 2001). It serve as an effective chemisorbent for chlorocarbons, organophosphorus compounds, and acidic gases like SO_2 and HCl (Klabunde et al., 1996; Stark et al., 1996; Mishakov et al., 2002). MgO also acts as an anti-bacterial agent against commonly found bacteria spores and viruses (Stoimenov et al., 2002, Lei et al., 2005). The other important environmental remediation aspect of MgO includes its potential to scavenge fluoride from drinking water and this property has been known for more than 70 years (Zettlemoyer et al., 1947; Fair and Geyer, 1954). MgO is suggested to be an attractive defluoridation agent due to its high adsorption capacity, non-toxic nature and limited solubility in water; several attempts are being made to improve the defluoridation performance of MgO (Rao and Mamatha, 2004; Sundaram et al., 2009). These studies demonstrated that defluoridation using MgO could be an effective alternative for Nalgonda technique and activated alumina based adsorption, which have been traditionally used in India for defluoridation process. However, it is known that higher surface area and increased adsorption capacities for different contaminants is possible when the MgO crystal size is in the nanometer scale and smaller the crystallite size, better is the adsorption efficiency (Stark et al., 1996; Nagappa and Chandrappa, 2007). The higher reactivity of smaller size MgO particles is not only because of the large specific surface area but also due to the high concentration of low-coordinated sites and structural defects on their surface (Mishakov et al., 2002). Thus, high surface area nanomaterials having a larger fraction of defect sites per unit area should be of interest as adsorbents in environmental remediation processes.

Realizing that the cost of synthesis, simplicity and morphological characteristics of nanoparticles to be important parameters for their use in commercial applications, it is imperative that a self-propagating combustion route offers the best choice (Aruna and Mukasyan, 2008). Such approaches involve the use of fuel (e.g. urea, glycine, alanine, hydrazide, etc.) to initiate decomposition reaction of precursor metal salt at high temperature. In one embodiment of this approach, nano MgO has been prepared by self-propagated combustion of magnesium nitrate in presence of glycine (Nagappa and Chandrappa, 2007). The nanoparticles prepared by this route, having a size of 12–23 nm,

* Corresponding author. Tel.: +91 44 2257 4208; fax: +9 44 2257 0545.
E-mail address: pradeep@iitm.ac.in (T. Pradeep).

0048-9697/$ – see front matter © 2010 Elsevier B.V. All rights reserved.
doi:10.1016/j.scitotenv.2010.01.062

Nomenclature

C_e	equilibrium concentration of the fluoride in the solution (mg l^{-1})
q_e	amount of fluoride removed from aqueous solution at equilibrium (mg g^{-1})
q_t	amount of fluoride adsorbed on the adsorbent surface at any time t (mg g^{-1})
q_p	calculated solid phase fluoride concentration at equilibrium (mg g^{-1})
k_1	pseudo-first-order rate constant of adsorption (min^{-1})
k_2	pseudo-second-order rate constant of adsorption (g mg^{-1} min^{-1})
t	reaction time (min)
K_F	Freundlich isotherm constant (mg g^{-1}) (mg l^{-1})$^{-1/n}$
K_S	Sips isotherm constant (l g^{-1})
q_L	monolayer capacity of Langmuir equation (mg g^{-1})
q_S	specific adsorption capacity of Sips equation at equilibrium (mg g^{-1})
n	Freundlich adsorption intensity
b_L	Langmuir isotherm constant (l mg^{-1})
m_S	Sips isotherm constant

exhibit 6 times increase in the fluoride uptake vis-à-vis the commercial MgO and could reduce the sludge volume by 90%.

Among the various available fuels, glycine is reported to be the best tested fuel for obtaining smaller size MgO nanoparticles (Aruna and Mukasyan, 2008). However, the self-propagating combustion synthesis using glycine as fuel has a number of difficulties: (i) vigorous reaction between magnesium nitrate and glycine leads to the generation of large quantity of combustion gases. The formed MgO nanoparticles being extremely fine, escape along with the gases, thereby reducing the yield significantly. Thus, a large-scale production requires complicated controlling mechanism (Mukasyan and Dinka, 2007). (ii) full or part replacement of costly fuel like glycine with alternate low cost fuel is more preferred to reduce the cost and increase commercial viability. The modified process, however, should not increase the particle size. Keeping these factors in mind, we have developed a novel method for the preparation of extremely small MgO nanoparticles and demonstrated its use for fluoride removal application. The said method consists of self sustained combustion of reaction mixtures such as magnesium nitrate, glycine, urea and cellulose. Glycine and urea were used as combustion fuels and cellulose was employed as metal holding template to prevent escape of nanoparticles from the reactor during combustion. It also helps in preventing agglomeration of the combustion product. Recent studies on the use of cellulose fibers as a metal holding template also suggest that it can act as in-situ reactor for making various metal and metal oxide nanoparticles by making use of its nano-porous structure and high oxygen density (Dong and Hinestroza, 2009; He et al., 2003). Besides, being a carbonaceous material it can also provide additional combustion energy to propagate the reaction.

In order to demonstrate the environmental remediation application of as-synthesized MgO nanoparticles, detailed adsorption studies were conducted taking fluoride as the model pollutant. Spectroscopic studies providing insight into the mechanism of fluoride uptake by NM have also been conducted. In addition to NM synthesis and demonstration of its defluoridation capacity, this paper also address on a practical issue of using MgO as an adsorbent in drinking water, i.e. alkaline pH of the treated water. To the best of our knowledge, no simple and user friendly solution exists to address this problem so far. A novel and simple adsorption based solution to bring down the pH to an acceptable limit (6.5–8.5) is proposed. We have also developed a household drinking water purification set-up and evaluated its performance for producing palatable water.

2. Materials and methods

2.1. Chemicals

Chemicals used in this study were of analytical grade. Magnesium nitrate, urea and potassium permanganate was procured from Ranbaxy Fine Chemicals Limited, India. Glycine was procured from SRL, India. A stock solution of 1000 mg l^{-1} fluoride was prepared from sodium fluoride (Ranbaxy, India) using distilled water. Required concentrations of the samples were prepared by serial dilutions of the stock solution.

2.2. Synthesis of nanomagnesia (NM)

Glycine and urea are the most commonly used fuels in most of the self sustained combustion reactions and the former is a better fuel for getting small size MgO nanoparticles (Aruna, and Mukasyan, 2008). But the cost of glycine is much higher than urea which makes the process more expensive. The other problem in using glycine as the sole fuel is the escape of particles along with the released combustion gases, which makes the recovery cumbersome. In order to address the above issues, a new approach has been tried by using a combination of fuels such as urea, glycine and cellulose. The main intention behind using cellulose was to act as a reaction mixture holding template and thereby prevent the agglomeration and escape of combustion products from the reaction vessel. In addition, it can also provide additional combustion energy to propagate the reaction. After many trials, an optimum glycine concentration of 0.6 M was used to minimize the fuel cost (compared to the stoichiometric concentration of 1.1 M glycine). A cheaper fuel, such as urea was added to the mixture to compensate for the fuel requirement so as to obtain enough combustion energy to propagate the reaction. Stoichiometric composition of metal nitrate and fuels is calculated based upon propellant chemistry. The fuel to oxidizer ratios (F/O) was calculated using the equation below (only urea and glycine were included in the calculation).

$$F/O = \left\{\frac{U_{MF}(1\times 4_C + 4\times 1_H + 2\times O_N + 1\times(-2)_O)}{N_{MF}\left(1\times 2_{Mg} + 2(1\times O_N + 3\times(-2)_O)\right)}\right\} + \left\{\frac{G_{MF}(2\times 4_C + 5\times 1_H + 1\times O_N + 2\times(-2)_O)}{N_{MF}\left(1\times 2_{Mg} + 2(1\times O_N + 3\times(-2)_O)\right)}\right\}$$

Where, G_{MF} is the molar fraction of glycine; U_{MF} is the molar fraction of urea, N_{MF} is the molar fraction of n1itrate. The F/O ratio was taken as 0.75. Addition of cellulose was fixed after few trails of the experiments. The possible combustion reactions of urea, glycine and cellulose with magnesium nitrate are illustrated in reactions R1 to R2. However, as of now, the exact details are unknown and more investigations are required to probe the same.

$$Mg(NO_3)_2\cdot 6H_2O_{(s)} + NH_2CONH_{2(s)} \rightarrow MgO_{(s)} + 8H_2O_{(g)} + CO_{2(g)} + 2N_{2(g)} + O_{2(g)} \quad (R1)$$

(Rao and Sunandana, 2008)

$$9Mg(NO_3)_2\cdot 6H_2O_{(s)} + 10NH_2CH_2-COOH_{(s)} \rightarrow 9MgO_{(s)} + 20CO_{(g)} + 14N_{2(g)} + 79H_2O_{(g)} \quad (R2)$$

(Nagappa and Chandrappa, 2007)

$$14Mg(NO_3)_2 \cdot 6H_2O_{(s)} + 10C_6H_{10}O_{5(s)} \rightarrow 14MgO_{(s)} + 14N_{2(g)} + 60CO_{2(g)} + 134H_2O_{(g)} \quad (R3)$$

In a typical synthesis process, magnesium nitrate, urea, glycine and cellulose fibers (Lenzing AG, India) were initially mixed and kept overnight. The weight ratio of magnesium nitrate:urea:glycine:cellulose used was 10.68:4.01:1.86:1.0. The mixture was then heated on a hot plate under stirring for 20 min to evaporate the excess water and was subsequently fired in a muffle furnace at 450 °C for 45 min. Combustion time of 45 min was used to completely burn the organic matter present in the product so as to get pure MgO. White aerogel kind of powder was formed in the reactor and the recovery of combustion product was almost 100%. The cost analysis shows that around 20% reduction of raw material cost could be achieved with this method (for cost details please refer to Table S1 in the Supplementary data).

2.3. Material characterization

The identification of the phase(s) of the as-prepared sample and fluoride reacted sample was carried out by X-ray powder diffraction (Bruker AXS, D8 Discover, USA) using Cu-Kα radiation at λ = 1.5418 Å. A scan step of 1 s and step size of 0.1 (in 2θ) was applied to record the patterns in the range from 10 to 90° (2θ). A software database published by the Joint Committee on Power Diffraction Standards (JCPDS) was used to analyze the X-ray diffractograms. Surface morphology, elemental analysis and elemental mapping studies were carried out using a Scanning Electron Microscope (SEM) equipped with Energy Dispersive Analysis of X-rays (EDAX) (FEI Quanta 200). High-Resolution Transmission Electron Microscopy (HRTEM) images of the sample were obtained with JEOL 3010 with a UHR polar piece. X-ray Photoelectron Spectroscopic (XPS) analysis was done using ESCA Probe TPD of Omicron Nanotechnology. Monochromatic Mg Kα was used as the X-ray source (hν = 1253.6 eV). Spectra in the required binding energy range were collected and an average was taken. Beam induced damage of the sample was reduced by adjusting the X-ray flux. Binding energy was calibrated with respect to C 1 s at 284.5 eV. The surface area, pore-size distributions, and micropore volume of as-synthesized NM were determined using a micropore analyzer (ASAP 2020, Micromeritics, USA).

2.4. Fluoride removal experiments

Batch reactions of NM with fluoride were carried out in 250 ml polypropylene conical flasks. The working volume of synthetic fluoride solution was taken as 100 ml and required quantities of NM dose were added. Immediately after the addition of NM, the flasks were kept for shaking at 160 ± 5 rpm in an orbital shaker (Riviera, India) at room temperature (30 ± 2 °C). Samples were withdrawn at pre-determined time intervals and analyzed for residual fluoride concentrations using a calibrated specific fluoride combination electrode (Cole-Parmer Instruments Co, USA) connected to a multimeter/data acquisition system (Keithley, 2700, USA). To each sample, ionic strength and pH adjusting buffer (TISAB III) was added in equal volumes (Agarwal, et al., 2003; Chidambaram, et al., 2003). Effect of contact time and initial fluoride concentration on fluoride uptake was studied at two different fluoride concentrations of 5 and 10 mg l^{-1}. Equilibrium studies were performed at neutral pH (7 ± 0.1) and at room temperature (30 ± 2 °C) by varying the concentrations of the fluoride solution over a wide range (5–200 mg l^{-1}). Effect of adsorbent dose (5–100 mg) was investigated at a pH of 7 ± 0.1 and fluoride concentration of 10 mg l^{-1}. Effect of pH on fluoride adsorption was carried out by varying the pH from 3 to 11. The initial pHs of the samples were adjusted using dilute NaOH or HCl.

2.5. pH control experiments

pH control experiments were conducted with the field water, which was initially subjected to fluoride treatment studies. The treated water was filtered and passed through a glass column packed with manganese oxide-supported-activated alumina at a flow rate of 3.7 ± 0.2 $m^3\ m^{-2}\ h^{-1}$. Manganese oxide coating on activated alumina surface was done by pore volume impregnation of activated alumina with potassium permanganate and its subsequent reduction with ethanol. Ethanol was added to the potassium permanganate-alumina mixture drop-wise under stirring for 15 min. The mixture was kept idle for 2 h and washed with distilled water and dried at 80 °C over night. The effluent solution was collected at various intervals and tested for pH using a calibrated pH meter (Cyberscan, Eutech Instruments, Singapore). The reuse potentials of this adsorbents were also tested by regenerating the already exhausted adsorbents with H_2SO_4 (0.25 N).

2.6. Household defluoridation unit (HDU)

The HDU consists of a 10 l bucket reactor fitted with a tap at the outlet. The reactor is followed by a vertical fixed-bed filter unit consisting of a 20 cm fine sand layer at the top (0.25–0.44 mm) and 20 cm manganese oxide-supported-activated-alumina layer at the bottom. A sieve on which a cotton cloth was placed to remove any suspended material was also attached at the top of the fixed-bed filter unit. The schematic of the experimental set-up is shown in Fig. 1. The reactor was operated in the batch mode. Required quantity of adsorbent (NM) was added to the fluoride contaminated water under stirring conditions, which was carried out by means of an electric mixing paddle and the stirring was continued for 60 min followed by 30 min settling. The supernatant water was then passed through a cotton cloth into the fixed-bed filter unit, where it percolates through sand and manganese oxide-supported-activated alumina bed at a flow rate of 3.7 ± 0.2 $m^3\ m^{-2}\ h^{-1}$ (empty bed contact time = 3 - 3.3 min). The sand

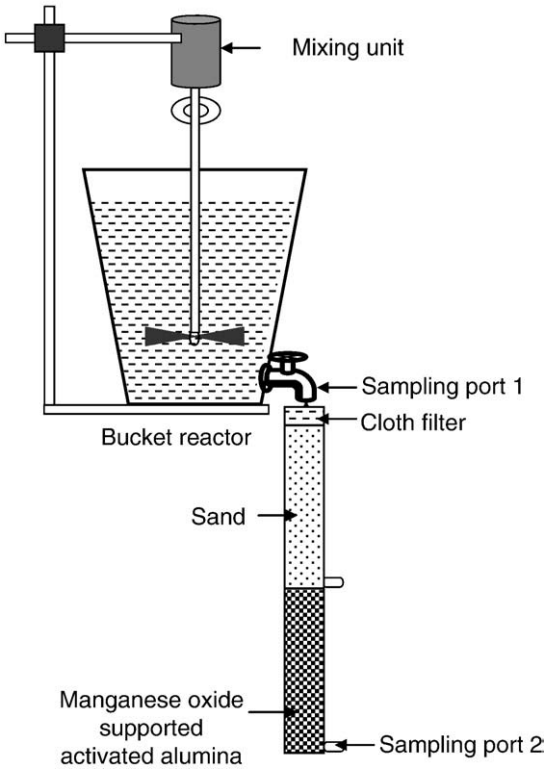

Fig. 1. Schematic of a household defluoridation unit (HDU).

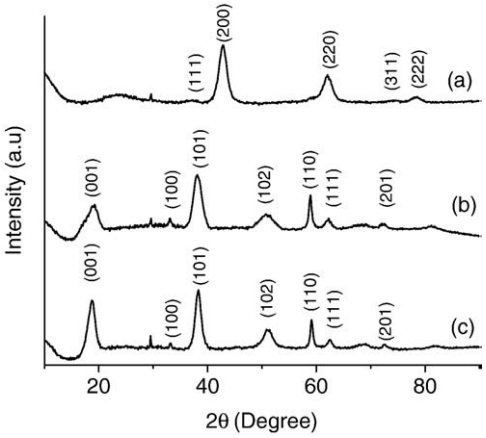

Fig. 2. XRD spectra of (a) as made NM (b) Hydrated NM (c) NM after reaction with 50 mg l^{-1} fluoride. The traces are shifted vertically for clarity.

filter bed acts as an extra safety device collecting any suspended matter, which might escape through the cloth filter. The sand bed also provides additional safety for bacterial removal. The prime purpose of manganese oxide-supported-activated alumina bed was to bring down the alkaline pH imparted by NM treated water to permissible levels (pH 6.5–8.5). It also provides additional safety against a wide spectrum of heavy metals (Dong, et al., 2003; Han et al., 2006; Maliyekkal et al., 2009). The mixing may be carried out manually in areas where electricity or cost is a concern.

3. Results and discussion

3.1. Material characterization studies

XRD analysis was performed to examine the crystal structure, size and phase purity of NM and fluoride reacted NM. The typical XRD patterns of these samples are shown in Fig. 2. The NM showed peaks corresponding to (111), (200), (220) and (222) planes, indicating the presence of cubic MgO and the peaks can be assigned to a pure phase of periclase MgO (PDF # 71-1176). The mean crystallite size calculated from the Scherrer formula shows that nanocrystals are of an average size of 6.9 nm. Fluoride (50 mg l^{-1}) reacted MgO samples showed XRD patterns corresponding to $Mg(OH)_2$ with peaks corresponding to brucite (PDF # 44-1482).

The SEM micrographs of freshly-prepared NM and fluoride reacted NM are shown in Fig. 3. NM powders look highly porous. The porous nature of the as-synthesized MgO can be attributed to the evolution of large amount of gases during the combustion reaction. SEM micrographs of fluoride sorbed NM and fluoride reacted NM have shown clear difference in the surface morphologies. After reaction with fluoride, porous nature of MgO was destroyed and a flower like structure was formed, this may be attributed to the hydration and subsequent formation of $Mg(OH)_2$. Fig. 4A shows a TEM micrograph of NM. The Fig. 4B shows an expanded image of an as-synthesized MgO nanoparticle. From these figures, we can see that the sizes of most particles are below 5 nm, which is in agreement with the mean crystallite size calculated from the Scherrer formula. A lattice image was clearly observed and the lattice spacing is matching with the (200)

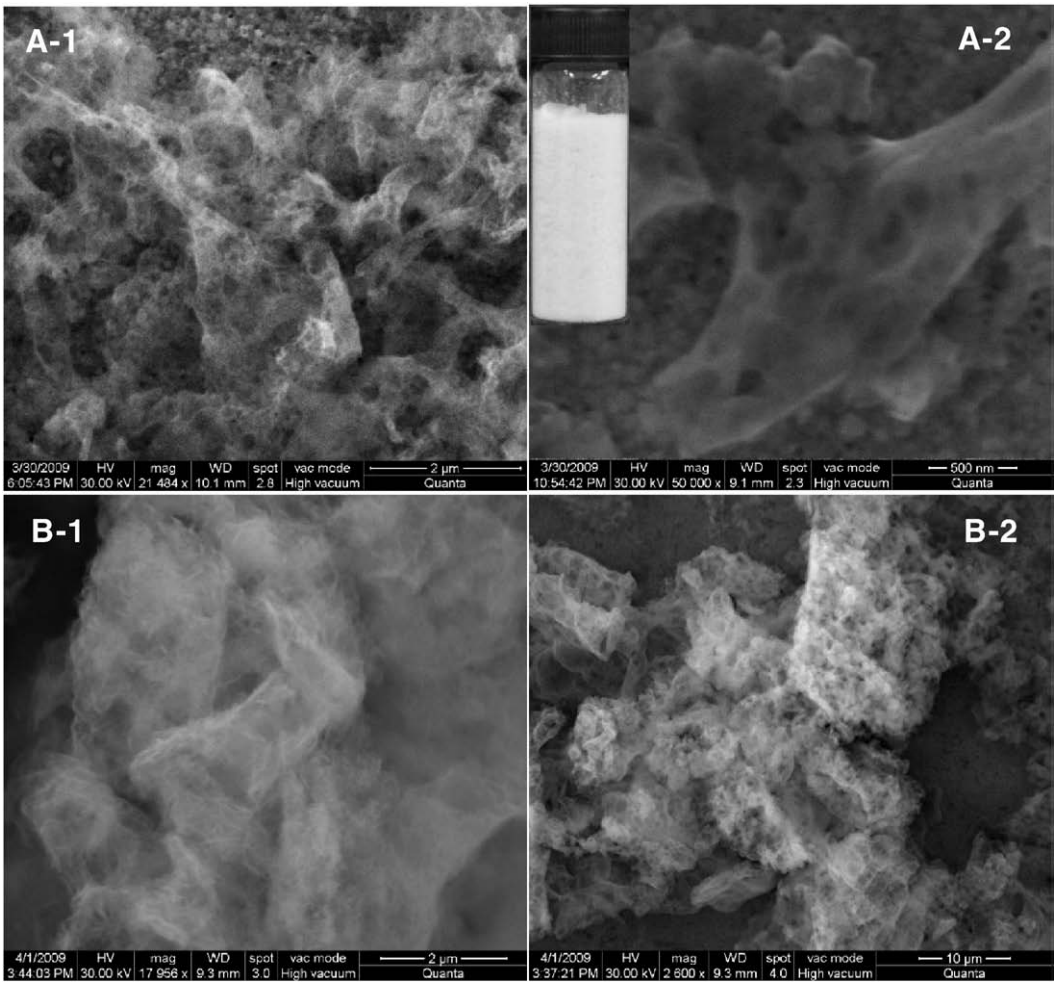

Fig. 3. SEM micrographs of (A–1, A–2) as-synthesized NM and (B–1, B–2) NM after reaction with fluoride. Inset of A–2 is a photograph of the as-synthesized NM.

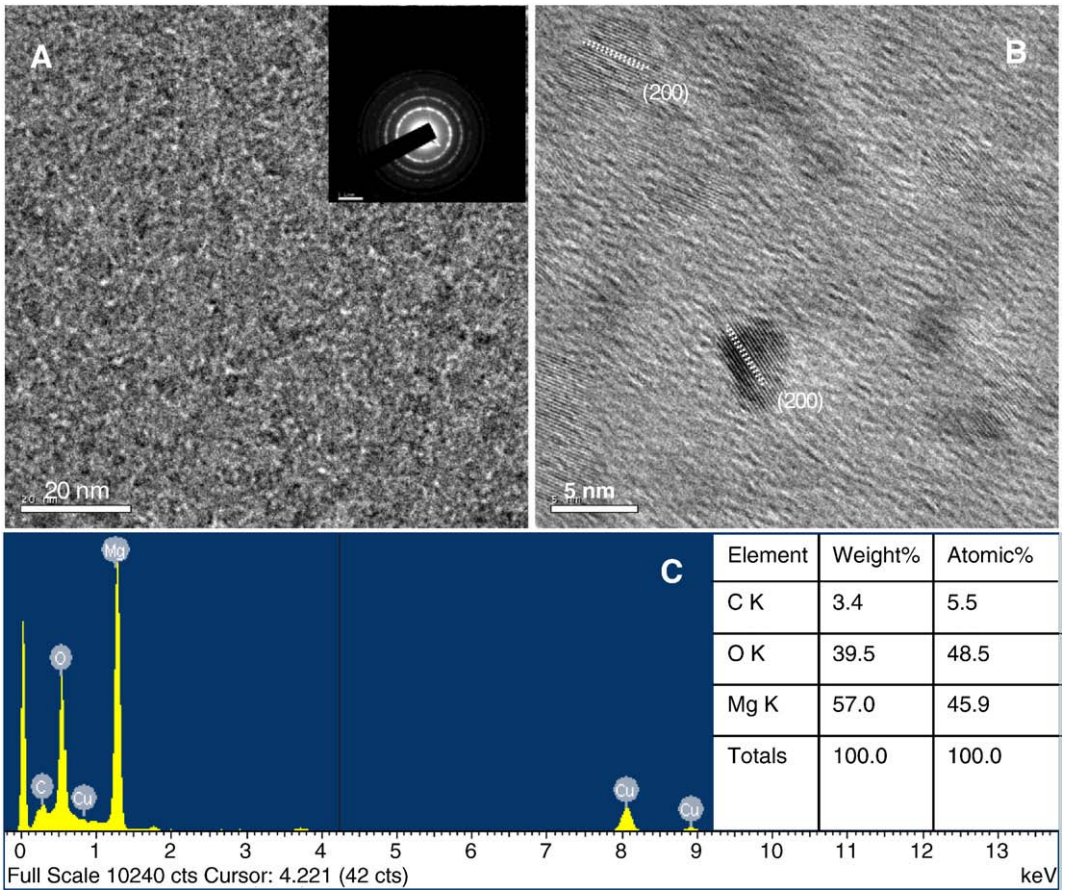

Element	Weight%	Atomic%
C K	3.4	5.5
O K	39.5	48.5
Mg K	57.0	45.9
Totals	100.0	100.0

Fig. 4. TEM images of (A) as-synthesized NM (inset: SAED pattern) (B) a particle from (A) is expanded (C) EDX spectrum of as-synthesized NM (inset: elemental composition of as-synthesized NM). Note that the grid used was carbon coated copper.

plane of periclase MgO. The EDX spectrum of MgO nanoparticles showed in Fig. 4C further confirms the formation of MgO.

Physical surface characteristics, BET specific surface area, micropore volume, and pore diameter of the as-synthesized NM were measured with low-temperature N_2 adsorption isotherm technique. The nitrogen adsorption and desorption isotherm plots are shown in Fig. S1 of Supplementary data. The BET (Brunauer, Emmett, and Teller) surface area and pore volume of adsorption (of pores less than 86.4 nm radius) were estimated to be 114.03 $m^2\ g^{-1}$ and 0.447 [$cm^3\ g^{-1}$], respectively. The BJH (Barret–Joyner–Halenda) average pore radius of desorption was calculated to be 5.9 nm.

3.2. Fluoride removal mechanism

Various mechanisms have been proposed for fluoride removal by MgO. Many previous researchers have described fluoride removal by chemisorption and the formation of MgF_2 (Zettlemoyer et al., 1947; Rao and Mamatha, 2004; Nagappa and Chandrappa, 2007). Booster et al. (2003) ascribed magnesia-fluoride reaction by isomorphic substitution of fluoride in brucite lattice. In this study, we have carried out various spectroscopic, microscopic and macroscopic studies to understand the existence and the chemical form of fluoride on the surface of NM. Initially, powder XRD patterns of NM and fluoride reacted NM were taken. The fluoride reacted NM showed peaks corresponding to $Mg(OH)_2$. No evidence of MgF_2 formation was observed at the concentration of fluoride studied. It is apparent that $Mg(OH)_2$ ($K_{sp} = 5.61 \times 10^{-12}$) has lower solubility product than MgF_2 ($K_{sp} = 5.16 \times 10^{-11}$) and hence, $Mg(OH)_2$ will be a preferred product than MgF_2 at lower concentration of fluoride (Booster et al., 2003). It may be noted that the theoretical maximum fluoride removal that can be achieved by precipitation of MgF_2 ($K_{SP} = 5.16 \times 10^{-11}$) is 8.9 mg l^{-1}. However, the experimental evidence shows that fluoride removal happens even at a level below 0.5 mg l^{-1}, this also disproves the formation of MgF_2 as the reason for fluoride removal at the fluoride concentration range studied. Hence, for further investigations, XPS analysis was carried out and the data are presented in Fig. 5. The F 1 s in XPS spectrum (Fig. 5c) at 683 eV clearly indicates the existence of fluoride on the surface. However, it is not present as magnesium fluoride (clear from XRD data) and therefore, one can attribute the fluoride removal thorough isomorphic substitution of hydroxyl groups by fluoride in brucite lattice. This reaction is possible since both the $F^-$and OH^-ions are iso-electronic in nature and of similar size and comparable ionic radii. From the analysis of detailed spectrum of Mg, F and O, we can see a clear shift in the peak position of Mg and F in presence of fluoride. This rules out the possibility of physisorption and supports a chemisorption mechanism as described above.

3.3. Fluoride removal studies

3.3.1. Effect of NM dose

The extent of fluoride adsorption by NM as a function of adsorbent dose was studied and the result is shown in Fig. 6. Amount of fluoride adsorbed increased with increase in NM dose from 5 to 50 mg and becomes fairly constant for any further increase in the NM dose. This can be attributed to the increase in the available reaction sites with increase in the NM dose (Ho et al., 1995; Sundaram et al., 2009). When the NM dose was further increased, there was less proportionate increase in adsorption. This may be because of the limitation of fluoride ions as compared to the NM sites available for the reaction (Kamble et al., 2007). Hence, the optimum NM dose was maintained as 50 mg.

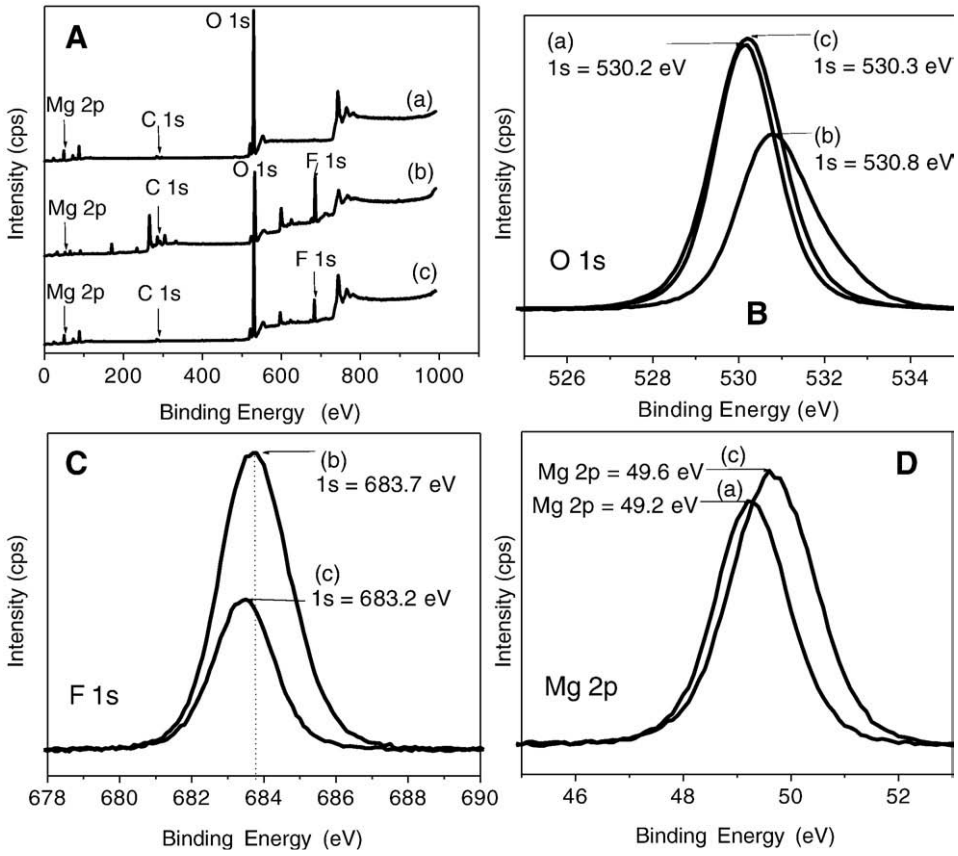

Fig. 5. XPS spectra of (a) hydrated NM, (b) MgF_2 (supplier: Leo Chem, Bangalore, India and (c) NM after reaction with 50 mg l^{-1} of fluoride. Various regions (O1s, F 1s and Mg 2p) are expanded.

3.3.2. Kinetic studies

Rate of adsorption is an important factor in any adsorption process. It varies with the surface and pore properties of the sorbent. In this study, batch fluoride adsorption kinetic studies were conducted using NM and the results are presented in Fig. 7 (A and B). NM has successfully removed fluoride within a short period and most of the fluoride removal took place in the first 15 min of contact time and the pseudo-equilibrium was reached in 90 min. To describe the kinetics of fluoride adsorption in a better manner, adsorption kinetics was analyzed using two reaction kinetic models, which included pseudo-first-order (Lagergren, 1898; Ho and McKay, 1998) and pseudo-second-order-equations (Ho and McKay, 2000). The mathematical representations of these models are as follows:

Pseudo-first-order equation:

$$q_t = q_e\left(1-e^{-k_1 t}\right) \tag{1}$$

Pseudo-second-order equation:

$$q_t = \frac{q_e^2 k_2 t}{1 + q_e k_2 t} \tag{2}$$

Where q_e and q_t are the adsorption capacity at equilibrium and at time t, respectively (mg g^{-1}). k_1 is the rate constant of pseudo-first-order adsorption (1 min^{-1}) and k_2 is the rate constant of pseudo-second-order adsorption (g mg^{-1} min^{-1}).

Estimation of kinetic parameters was carried out by non-linear least-squares method using Microsoft Excel® with solver add-on option (Ho, 2006). The kinetic plots generated by pseudo-first-order and pseudo-second-order-equations along with the experimental kinetic plots are given in Fig. 7A and B, respectively. The kinetic parameters obtained from these model fits are summarized in Table 1. From the table, it is clear that the kinetic data fit well with the pseudo-second-order equation as it is evident from the low RMSE (Root Mean Squared Error) and Chi-square value (χ^2). The Chi-square test statistic also shows that the predicted data from the model falls into above 99% confidence level. From this table, it can also be seen that the rate coefficient obtained is concentration dependent. Many adsorption studies using metal oxides conducted by previous researchers have observed an increasing trend in adsorption rate at higher concentrations of fluoride (Das et al., 2005; Ghorai and Pant, 2005).

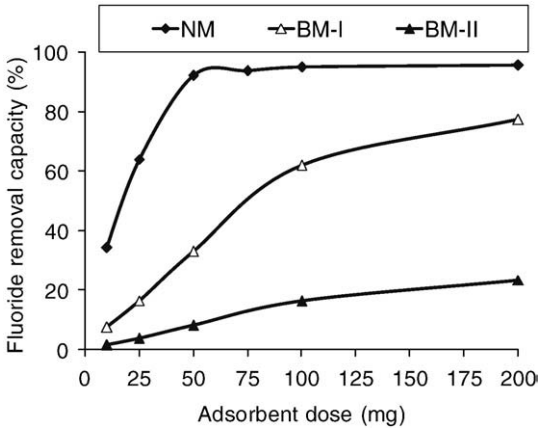

Fig. 6. Effect of adsorbent dose on fluoride removal (initial fluoride conc. = 10 mg l^{-1}). Legends—NM: as-synthesized nano MgO; BM-1: MgO light (Thomas backer limited, Mumbai, India); BM-II: bulk MgO (Commercial grade).

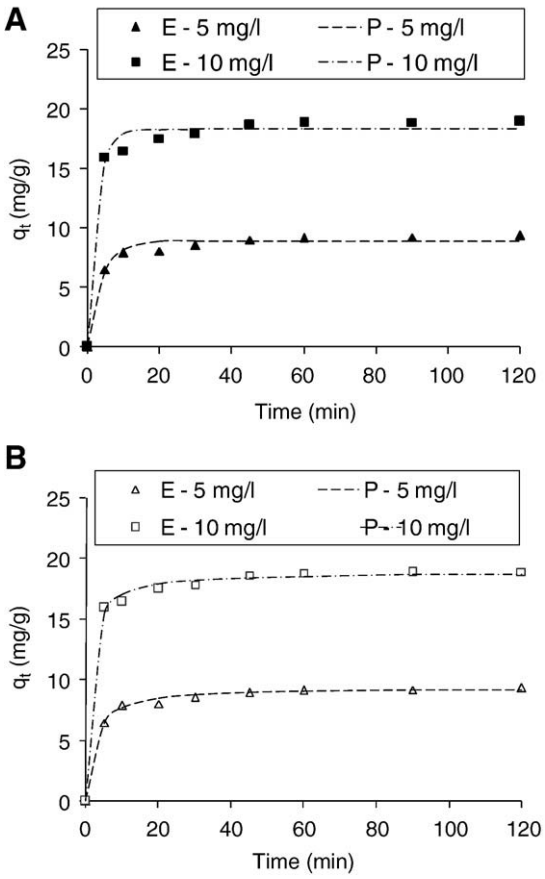

Fig. 7. Comparison of (A) pseudo-first-order and (B) pseudo-second-order kinetic plots with experimental data for adsorption of fluoride by NM (E—experimental; P—predicted).

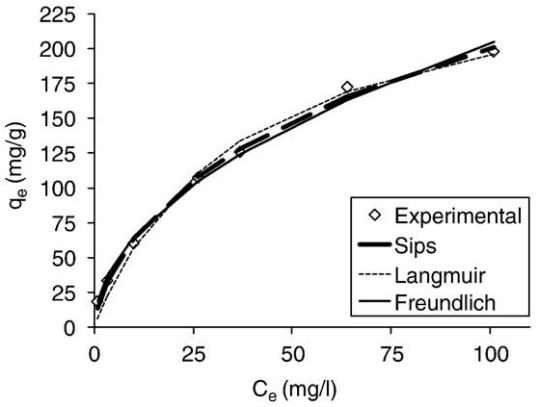

Fig. 8. Comparison of various isotherm models for fluoride adsorption onto NM (temperature — 30 ± 2 °C).

Table 2
Isotherm parameters obtained for the adsorption of fluoride by NM.

Isotherm models	Model parameters	Estimated parameters
Freundlich	K_F (mg g^{-1}) (mg l^{-1})$^{-1/n}$	20.66
	n	2.01
	RMSE	5.16
	χ^2	1.67
Langmuir	q_L (mg g^{-1})	267.82
	b (l mg^{-1})	0.027
	RMSE	7.37
	χ^2	34.6
Sips	q_S (mg g^{-1})	515.21
	K_S (l g^{-1})	0.005
	m_S	0.65
	RMSE	3.86
	χ^2	2.22

3.3.3. Adsorption equilibrium

Adsorption capacity is one of the basic parameters required for the design of any batch or fixed-bed adsorption system. The equilibrium adsorption study of fluoride by NM was carried out at 30 ± 2 °C and neutral pH. The initial fluoride concentration was varied over a wide range in order to attain complete exhaustion of the adsorbent. The data obtained from this study are analyzed with the help of various isotherm models, including the well-known Langmuir, Freundlich, and Sips isotherms. The mathematical representations of these models are given in Eqs. 3–5 and the details are given elsewhere (Freundlich, 1906; Langmuir, 1918; Sips, 1948).

Langmuir model:

$$q_e = \frac{q_L b_L C_e}{1 + b_L C_e} \tag{3}$$

Freundlich model:

$$q_e = K_F C_e^{1/n} \tag{4}$$

Sips model:

$$q_e = \frac{q_{mS}(K_S C_e)^{m_s}}{1 + (K_S C_e)^{m_s}} \tag{5}$$

Where q_e is the amount of solute adsorbed per unit weight of adsorbent at equilibrium (mg g^{-1}); C_e is equilibrium concentration of the adsorbate in the solution (mg l^{-1}); K_F is the Freundlich isotherm constant [(mg g^{-1}) (mg l^{-1})$^{-1/n}$]; q_L, and q_S represent maximum specific uptake capacities at equilibrium of Langmuir and Sips isotherms, respectively (mg g^{-1}); b_L, and K_S, are the Langmuir and Sips isotherm constants, respectively (l mg^{-1}); n_F, and m_S are Freundlich, and Sips isotherm exponents, respectively.

Fig. 8 shows the isotherm plots obtained for the adsorption of fluoride by NM. The estimated isotherm parameters from these model fits are given in Table 2. The experimental data fitted relatively well with Freundlich model, which is evident from the low RMSE and χ^2 values. The fit shows more than 95% confidence level. The predicted K_F, the maximum adsorption capacity, value of NM is 20.66 (mg g^{-1}) (mg l^{-1})$^{-1/n}$.

Table 1
Pseudo-first-order and pseudo-second-order rate parameters obtained for the adsorption of fluoride by NM.

Fluoride conc.(mg l^{-1})	Pseudo-first-order rate parameters				Pseudo-second-order rate parameters			
	k_1 (l min^{-1})	q_e (mg g^{-1})	RMSE	χ^2	k_2 (g mg^{-1} h^{-1})	q_e (mg g^{-1})	RMSE	χ^2
5.05	0.25	8.89	0.37	0.14	0.047	9.39	0.15	0.033
10.15	0.36	18.31	0.65	0.21	0.044	18.9	0.29	0.044

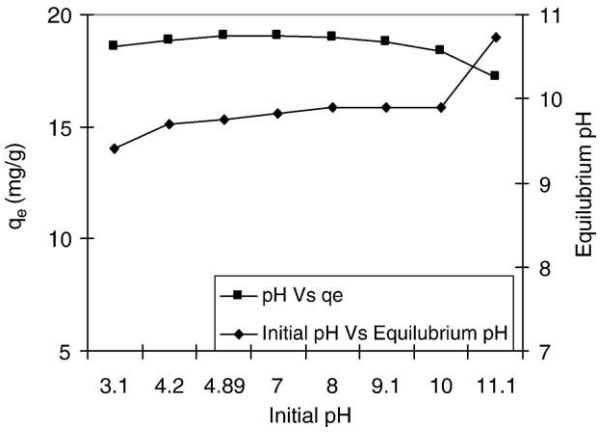

Fig. 9. Effect of pH on fluoride adsorption by NM (initial fluoride conc. = 10 mg l^{-1}, temperature—30 ± 2 °C).

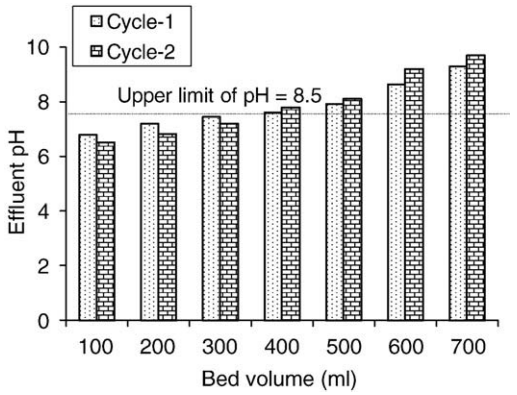

Fig. 11. Hydroxyl ion uptake capacity of manganese oxide-supported-activated alumina.

3.3.4. Effect of pH

Influence of pH on fluoride adsorption by NM was investigated and the data are shown in Fig. 9. Fluoride adsorption by NM is less sensitive to pH variations. At higher pH value, a slight decrease in fluoride removal was observed. This reduction in fluoride removal capacity at alkaline pH ranges may be attributed to the competition from the negatively charged OH^- ions (Ghorai and Pant, 2005; Raichur and Basu, 2001). Since, NM surface has a net positive charge at pH below pH_{zpc} (the reported pH_{zpc} value of magnesium oxide is 12.4 (Fierro, 2006), the possibility of electrostatic repulsion between fluoride ion and magnesia surface can be ruled out.

3.3.5. Effect of co-existing ions

Contaminated groundwater usually contains several other co-existing ions along with fluoride, which may compete with fluoride for the active adsorption sites. Hence, it is imperative to investigate the possible interference of these ions (HCO_3^-, Cl^-, NO_3^-, SO_4^{2-}, PO_4^{3-}, Ca^{2+}, Mg^{2+}, Fe^{3+} and Mn^{2+}) on fluoride removal by NM. This is essential to decide the suitability of NM for field applications. Fig. 10A shows the effect of various co-existing anions on fluoride removal by NM. The results show that most of the ions have little effect on fluoride removal by NM, comparing over the normal ion concentration range found in ground water. However, the presence of the HCO_3^- and NO_3^-, and higher concentrations of phosphate (>10 mg l^{-1}) affected the fluoride removal potential of NM. The results indicated that phosphate is the greatest competitor for fluoride followed by bicarbonate and nitrate. However, from a practical point of view, the interference by phosphate is not a serious concern because the phosphate content in groundwater is usually much lesser than 10 mg l^{-1}.

Fig. 10B shows the effect of various commonly found cations on fluoride removal by NM. As evident from this figure, magnesium and calcium did not reduce the adsorption capacity of NM. In fact a slight increase in adsorption capacity was observed with higher concentration of these ions. This slight increase in adsorption may be attributed to the increase in surface positive charges which help to attract negatively charged ions onto various metal oxide surfaces. Similar phenomenon has been observed in the case of other anions also (Takamatsu et al., 1985; Kundu and Gupta, 2006). Unlike calcium and magnesium, an interesting trend in fluoride removal was observed due to the presence of Mn^{2+} and Fe^{3+}. At lower concentration of these ions, an increase in fluoride removal was observed. Upon increasing the concentration above 25 mg l^{-1}, fluoride removal capacity is gradually reduced and at 200 mg l^{-1}, around 5–10% reduction in fluoride removal efficiency was observed.

3.4. pH control studies

In field conditions, the major limitation of using MgO as adsorbent is the high alkaline pH of the treated water. Hence, the treated water pH must be brought down to a limit less than 8.5. In this study, a user friendly method was proposed by making use of the OH^- ion removal capacity of metal oxide adsorbents. In this study, manganese oxide-coated-activated alumina was used based on the previous knowledge of these materials that it can adjust the pH to a neutral value, since it

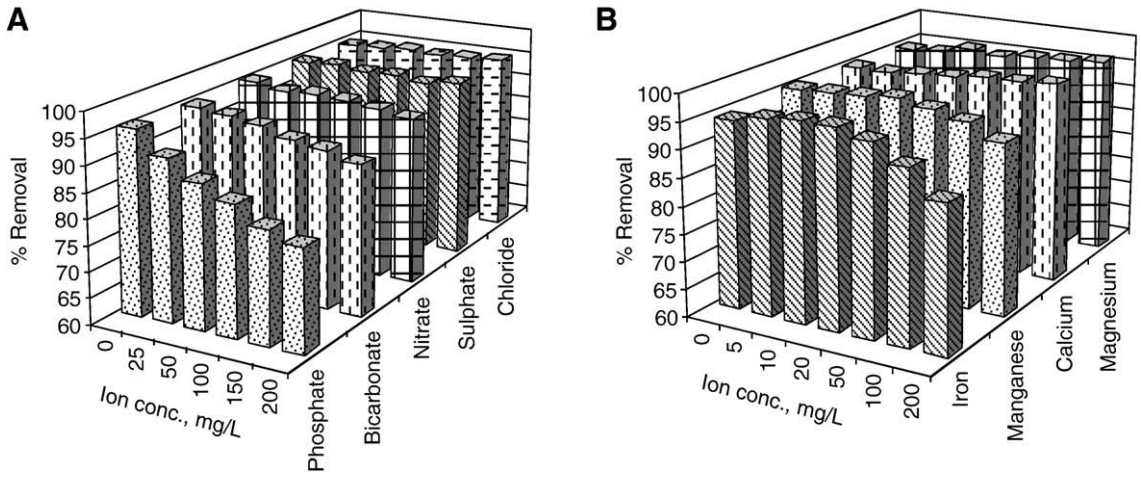

Fig. 10. Effect of various background (A) anions and (B) cations on the fluoride removal capacity by NM (initial fluoride concentration = 10.0 mg l^{-1}, pH 7 ± 0.1).

Table 3
Physicochemical characteristics of raw and treated water.

Parameters	Influent water (Kotlapalli Panchayath Puttaparthi , Andhra Pradesh, India)	Treated water	
		Sampling port 1	Sampling port 2
pH @ 25 °C	8.01	10.1	7.79
Fluoride	2.34	0.38	<0.1
Total alkalinity (as $CaCO_3$)	217	326	61
Total hardness (as $CaCO_3$)	178	303	28
Conductivity @ 25 °C	565 μmhos cm^{-1}	658 μmhos cm^{-1}	216 μmhos cm^{-1}
Organic carbon	<0.5	<0.5	<0.5
Total dissolved solids	384	412	142
Calcium (as Ca^{2+})	36	8	1.6
Magnesium (as Mg^{2+})	22	69	5.9
Sulphate (as SO_4^{2-})	25	14	4.7
Chloride (as Cl^{-1})	13	13	11.6
Phosphate (as PO_4^{3-})	<0.02	<0.02	<0.02
Iron (as Fe^{3+})	<0.001	<0.001	<0.001
Nitrate (as NO_3^-)	38.9	44.5	37.4
Turbidity (as NTU)	0.2 NTU	-	0.1 NTU
Silica (as SiO_2)	47.4	0.69	0.03
Manganese	<0.001	<0.001	<0.03

Note: All parameters are expressed in mg l^{-1}, except pH, turbidity and conductivity.

has a nearly neutral pHzpc (7.7 ± 0.2) (Maliyekkal et al., 2006; Tripathy and Raichur, 2008). The second reason for selecting this material was its ability to remove wide range of ions including heavy metals. Fig. 11 shows the OH^- removal capacity of manganese oxide-supported-activated alumina. The results show that manganese oxide-supported-activated alumina could reduce the pH of the fluoride treated water to an acceptable limit. The regeneration capacity of the adsorbents was also found to be excellent and no significant reduction in performance was observed up to 2 cycles of adsorption process, which makes the sorbent more economical and viable option for field conditions.

3.5. Household defluoridation unit (HDU)

A 10 l capacity batch bucket reactor followed by a post treatment unit, as described in the experimental section (see Fig. 1 for a schematic) was used to treat the fluoride contaminated water. The study was carried out with field water samples collected from Kotlapalli Panchayath of Puttaparthi, Anantapur district, Andhra Pradesh, India—a fluoride affected area. The water quality characteristics of theses samples before and after treatment are listed in Table 3. From the table it is clear that both fluoride and alkaline pH of the fluoride treated water meet the safe drinking water standards. It is also worth noting that the TDS (Total Dissolved Solids) level of the effluent water was considerably reduced and the treatment process did not add any unwanted chemicals into the effluent.

4. Conclusions

From the study of practical applicability of nano MgO in removing fluoride from drinking water, it can be concluded that:

- Ultra fine MgO nanoparticles (3–7 nm) were synthesized through a novel self sustained combustion route. The flying off of the combustion product from the reaction vessel was completely arrested and thereby 100% recovery of the product, without additional product recovery mechanism, was achieved.
- The raw material cost of the combustion reaction could be brought down by ~20% viz a viz to a previously reported method of Nagappa and Chandrappa (2007).
- Nano MgO is a potential candidate for defluoridation of contaminated drinking water. The defluoridation efficiency of nano MgO was found to be independent of normal pH variations found in drinking water.
- The kinetics of fluoride removal by nano MgO followed pseudo-second-order equation. Among the various adsorption isotherms tested, Freundlich model described the equilibrium data well. The study on the effect of various co-existing ions indicated that fluoride removal by nano MgO is a selective process.
- The proposed HDU was effective in treating fluoride and controlling the pH well below the permissible limit. The TDS level of the raw water could be considerably reduced after the treatment. Consequently, the system may be used as an effective alternative for the defluoridation of contaminated drinking water.

Acknowledgements

Authors thank Mr. Sundara Krishnaswami and his team for financial support. Instrumentation was supported by the Department of Science and Technology (DST), India through the Nano Mission. Analyses of field and treated water samples were carried out by SGS India Pvt. Ltd. Laboratory, Chennai, India. We thank Lenzing AG for the generous gift of cellulose samples.

Appendix A. Supplementary data

Supplementary data associated with this article can be found, in the online version, at doi:10.1016/j.scitotenv.2010.01.062.

References

Agarwal M, Rai K, Shrivastav R, Das S. Deflouridation of water using amended clay. J Clean Prod 2003;11(4):439–44.
Aruna ST, Mukasyan AS. Combustion synthesis and nanomaterials. Curr Opin Solid State Mater Sci 2008;12(3–4):44–50.
Booster JL, Van Sandwijk A, Reuter MA. Conversion of magnesium fluoride to magnesium hydroxide. Miner Eng 2003;16:273–81.
Chidambaram S, Ramanathan AL, Vasudevan S. Fluoride removal studies in water using natural materials: technical note. Water SA 2003;29(3):339–44.
Das N, Pattanaik P, Das R. Defluoridation of drinking water using activated titanium rich bauxite. J Colloid Interface Sci 2005;292:1–10.
Ding Y, Zhang G, Wu H, Hai B, Wang L, Qian Y. Nanoscale magnesium hydroxide and magnesium oxide powders: control over size, shape, and structure via hydrothermal synthesis. Chem Mater 2001;13:435–40.
Dong H, Hinestroza JP. Metal nanoparticles on natural cellulose fibers: electrostatic assembly and in situ synthesis. ACS Appl Mater Interfaces 2009;1(4):797–803.
Dong D, Hua X, Li Y, Zhang J, Yan D. Cd adsorption properties of components in different freshwater surface coatings: the important role of ferromanganese oxides. Environ Sci Technol 2003;37:4106–12.
Fair GM, Geyer JC. Water supply and waste-water disposal. New York: John Wiley & Sons; 1954. p. 632.
Fierro JLG. Metal oxides: chemistry and applications. USA: CRC Press; 2006. p. 4.
Freundlich HMF. Über die Adsorption in Lösungen. Z Phys Chem 1906;57:385–470.
Ghorai S, Pant KK. Equilibrium, kinetics and breakthrough studies for adsorption of fluoride on activated alumina. Sep Purif Technol 2005;42:265–71.
Han R, Zoua W, Zhang Z, Shi J, Yang J. Removal of copper(II) and lead(II) from aqueous solution by manganese oxide coated sand I. Characterization and kinetic study. J Hazard Mater 2006;B137:384–95.
He J, Kunitake T, Nakao A. Facile in situ synthesis of noble metal nanoparticles in porous cellulose fibers. Chem Mater 2003;15(23):4401–6.
Ho YS, McKay G. Kinetic models for the sorption of dye from aqueous solution by wood. Process Saf Environ Prot 1998;76(B2):183–91.
Ho YS. Second-order kinetic model for the sorption of cadmium onto tree fern: a comparison of linear and non-linear methods. Water Res 2006;40:119–25.
Ho YS, McKay G. The kinetics of sorption of divalent metal ions onto sphagnum moss peat. Water Res 2000;34:735–42.
Ho YS, Wase DAJ, Forster CF. Batch nickel removal from aqueous solution by sphagnum moss peat. Water Res 1995;29(5):1327–32.
Kamble SP, Jagtap S, Labhsetwar NK, Thakare D, Godfrey S, Devotta S, et al. Defluoridation of drinking water using chitin, chitosan and lanthanum-modified chitosan. Chem Eng J 2007;129(1–3):173–80.
Klabunde KJ, Stark JV, Koper O, Mohs C, Park DG, Decker S, Jiang Y, Lagadic I, Zhang D. Nanocrystals as stoichiometric reagents with unique surface chemistry. J Phys Chem 1996;100:12142–53.
Kundu S, Gupta AK. Adsorptive removal of As(III) from aqueous solution using iron oxide coated cement (IOCC): evaluation of kinetic, equilibrium and thermodynamic models. Sep Purif Technol 2006;51:165–72.

Lagergren S. Zur theorie der sogenannten adsorption gelöster stoffe. K Sven Vetensk akad Handl 1898;24:1–39.
Langmuir I. The adsorption of gases on plane surface of glass, mica and platinum. J Am Chem Soc 1918;40:1361–403.
Lei H, Dianqing LI, Yanjun L, Evans DG, Xue D. Influence of nano-MgO particle size on bactericidal action against *Bacillus subtilis* var. niger. Chin Sci Bull 2005;50:514–9.
Maliyekkal SM, Sharma AK, Philip L. Manganese oxide coated alumina: a promising sorbent for defluoridation of water. Water Res 2006;40(19):3497–506.
Maliyekkal SM, Philip L, Pradeep T. As(III) Removal from drinking water using manganese oxide-coated-alumina: performance evaluation and mechanistic details of surface binding. Chem Eng J 2009;153(1–3):101–7.
Mishakov IV, Betilo AF, Richards RM, Chesnokov VV, Vladimir V, Zaikovskii I, et al. Nanocrystalline MgO as a dehydrohalogenation catalyst. J Catal 2002;206:40.
Mukasyan AS, Dinka P. Apparatus for synthesizing nanopowder, has carrier substrate, solution applicator, dryer and combustion chamber having ignition source for igniting impregnated carrier substrate to initiate combustion synthesis. 2007. PCT application WO2007019332-A1.
Nagappa B, Chandrappa GT. Mesoporous nanocrystalline magnesium oxide for environmental remediation. Microporous Mesoporous Mater 2007;106(1–3):212–8.
Rao SM, Mamatha P. Water quality in sustainable water management. Curr Sci 2004;87:942–7.
Rao KV, Sunandana CS. Structure and microstructure of combustion synthesized MgO nanoparticles and nanocrystalline MgO thin films synthesized by solution growth route. J Mater Sci 2008;43:146–54.
Raichur AM, Basu MJ. Adsorption of fluoride onto mixed rare earth oxides. Sep Purif Technol 2001;24:121–7.
Sips R. Structure of a catalyst surface. J Chem Phys 1948;16:490–5.
Stark JV, Park DG, Lagadic I, Klabunde KJ. Nanoscale metal oxide particles/clusters as chemical reagents. Unique surface chemistry on magnesium oxide as shown by enhanced adsorption of acid gases (sulfur dioxide and carbon dioxide) and pressure dependence. Chem Mater 1996;8(8):1904–12.
Stoimenov PK, Klinger RL, Marchin GL, Klabunde KJ. Metal oxide nanoparticles as bactericidal agents. Langmuir 2002;18:6679–86.
Sundaram CS, Viswanathan N, Meenakshi S. Defluoridation of water using magnesia/chitosan composite. J Hazard Mater 2009;163(2–3):618–24.
Takamatsu T, Kawashima M, Koyama M. The role of Mn^{+2}-rich hydrous manganese oxide in the accumulation of arsenic in lake sediments. Water Res 1985;19(8):1029–32.
Tripathy SS, Raichur AM. Abatement of fluoride from water using manganese dioxide-coated activated alumina. J Hazard Mater 2008;153(3):1043–51.
Zettlemoyer AC, Zettlemoyer EA, Walker WC. Active magnesia. II. Adsorption of fluoride from aqueous solution. J Am Chem Soc 1947;69:1312–5.